

UVM ScholarWorks

Lift & Drag Effects of a Variable-Angle Winglet System

Item Type	undergraduate thesis
Authors	Newman, Dante M
Download date	2026-06-08 13:36:07
Item License	http://creativecommons.org/licenses/by-nc-nd/3.0/
Link to Item	https://hdl.handle.net/20.500.14849/5276

Lift & Drag Effects of a Variable-Angle Winglet System

Dante Newman

Department of Mechanical Engineering
College of Engineering & Mathematical Sciences
The University of Vermont

April 30, 2020

Abstract

Winglets are systems that are used on aircraft to reduce drag and ultimately save money on fuel and pollution costs. A winglet exists on the end of a wing to reduce the amount of drag that affects each wing during flight. In 2020, these winglet systems are fixed and vary between aircraft based on different flight and geometry characteristics. The result of this is that each winglet is only optimal at a single design point or a single flight scenario. A variable-angle winglet system would allow the winglet to be optimal at multiple design points. In this experiment, a variable-angle winglet system is investigated based on different angles of attack, altitudes, and speeds. The results are found using computational fluid dynamics and wind tunnel testing. In the preliminary experiments it was found that the differences in air speed, altitude, and pitch for each flight condition affect the optimal cant angle significantly. The significance demonstrates the practicality of further research regarding potential prototyping and implementation.

Nomenclature

A = wing area (m^2)

D = characteristic length (m)

Re = Reynolds number (-)

g = acceleration due to gravity ($9.81 \frac{m}{s^2}$)

h = height of manometer fluid (m)

q = kinetic energy per unit volume ($\frac{kg}{ms}$)

α = angle of attack ($^\circ$)

μ = dynamic viscosity ($\frac{m^2}{s}$)

ϕ = angle of wing relative to vertical ($^\circ$)

C_D = coefficient of drag (-)

C_L = coefficient of lift (-)

F_D = force of drag (N)

F_L = force of lift (N)

P_{atm} = atmospheric pressure (Pa)

P_i = pressure at tap inlet (Pa)

P_∞ = pressure upstream of test section (Pa)

S_w = wing surface area (m^2)

U_∞ = velocity of fluid upstream of test section ($\frac{m}{s}$)

h_{atm} = height of manometer at atmospheric pressure tap (m)

h_i = height of manometer at inlet tap (m)

h_∞ = height of manometer upstream of test section (m)

ρ_a = density of air ($1.225 \frac{kg}{m^3}$)

ρ_w = density of water ($998 \frac{kg}{m^3}$)

Contents

1	Objective & Introduction	6
1.1	Objective	6
1.2	Introduction	6
1.2.1	Lift & Drag	6
1.2.2	Winglet Systems	8
1.2.3	Data Analysis	11
2	Models	12
2.1	Computational Test	12
2.1.1	Winglet Designs	12
2.1.2	Physics Model	18
2.1.3	Domain & Boundary Conditions	18
2.1.4	Numerical Models	20
2.2	Wind Tunnel Test	20
3	Methods & Measurements	21
3.1	Methods	21
3.1.1	Computational Test Methods	21
3.1.2	Wind Tunnel Test Methods	24
3.2	Measurements	26
3.2.1	Computational Test Measurements	26
3.2.2	Wind Tunnel Test Measurements	26
4	Calculations & Results	27
4.1	Calculations	27

4.1.1	Computational Test Calculations	27
4.1.2	Wind Tunnel Test Calculations	32
4.2	Results	33
4.2.1	Computational Test Results	33
4.2.2	Wind Tunnel Test Results	40
5	Conclusions	41
6	Future Work	42
7	Appendix	44
7.1	Pressure Map Along Wing Cross-section	44
7.2	Computational Journal File	45
7.3	Wind Tunnel Data	46
8	Acknowledgements	47

1 Objective & Introduction

1.1 Objective

The objective of this experimental study is to build off of the theoretical data proposed by Guerrero et al. in a previous study conducted at the University of Genoa in 2018. The result of this study was theoretical and computational data suggesting a benefit of winglet angle variation on commercial aircraft.¹ The article suggests a physical model be produced and tested in a wind tunnel analysis. Along with this, a redone computational analysis is to be conducted for verification purposes. The end result of this study will be a comparison of the two analyses and further flight condition modeling. This will provide a suggestion as to whether further, more detailed testing should occur.

1.2 Introduction

1.2.1 Lift & Drag

Lift and drag are phenomena that occur constantly in wing systems on aircraft. These forces are seen on not just wing systems, but across all airfoils. The relationship between the lift and drag on a wing is what allows it to support the weight of a fuselage and engines in order to function properly. Both lift and drag are the resultant forces of an object within a flow field and can be measured accordingly. They are caused by the momentum fluxes of the flow in different directions and by the different pressure variations around the object.² Lift and drag forces can be utilized for different purposes and this experiment will help better understand how each can be applied to a variable-angle winglet system. An example of a current winglet system can be seen in Figure 1.

In terms of fundamental physics, lift is the reactive force on an object that is perpen-



Figure 1: Example of Winglet Seen at End of Wing³

pendicular to the streamwise direction of the flow. On a particular aircraft, this is seen as the upwards force that keeps the plane aloft, with the use of the wings. There is also a smaller lift effect that occurs on the winglet of a wing system that does two things. It firstly sees the forces from the winglets being directed inward and acting as a stabilizing force. This force works with the rudder to make sure the plane does not yaw. It secondly sees the effect of wake vortices be drastically reduced. The vortices are still present and still increase with airspeed, however their magnitudes are reduced significantly.⁴ The fundamental design of the winglet system aims to maximize these benefits while seeking to reduce manufacturing and maintenance costs.

Drag is the reactive force on an object that occurs parallel to the streamwise flow velocity. This force is seen as the force opposing forward motion on aircraft systems. This force exists due to two things. First is the pressure differentials caused by the aircraft surfaces subjected to the flow field (pressure drag). Second is the friction emanating from the surfaces parallel to the flow with certain material properties (friction drag).⁵ While a significant proportion

of the surface area of an aircraft exists in the body of the plane, the wings and winglets also contribute to the drag. To what degree depends on numerous factors including relative airspeed, angle of attack, and winglet angle.⁶ A visual representation of these forces can be seen in Figure 2.

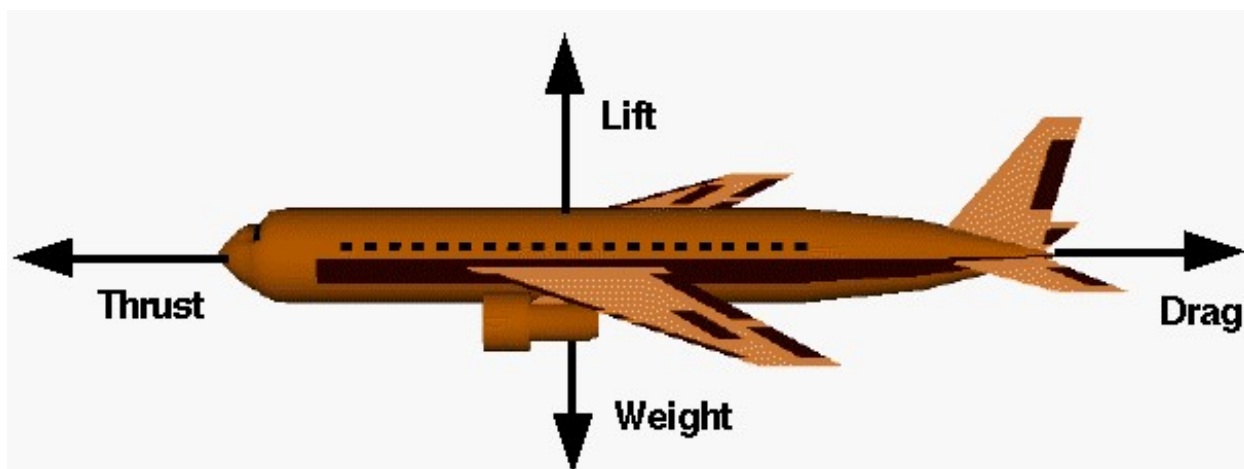


Figure 2: Forces on an Airplane During Flight⁷

1.2.2 Winglet Systems

On most jets and airplanes, winglet systems are designed to produce optimal drag minimization during level cruise at high altitude. This is the case because aircraft will spend a vast majority of their flight time at cruising altitude and level flight. Planes designed for short haul flights give more consideration to minimizing wingtip vortex generation because of how frequently they are taking off and landing.⁸ The larger the vortex generated, the longer it takes for the vortex to dissipate and the air be smooth enough to be deemed safe for a following aircraft to pass through. The addition of winglet systems does not entirely solve this problem, but it does significantly improve it. A visual depiction of how these systems affect downstream flow can be seen in Figure 3.



Figure 3: Effects of Adding A Winglet⁹

As previously stated, winglet systems are designed to reduce drag and wingtip vortices that emanate from the ends of aircraft wings as they fly through the air. These systems, as of now, are only commercially available as fixed-angle winglets, which are designed for a single optimal flight condition.¹⁰ The addition of these winglet systems ultimately make the aircraft more efficient. While what exists currently has proven beneficial on many fronts, there is more improvement that can be done, as these systems are not optimal for 100% of flight duration.¹¹ There are numerous parameters in which a winglet can be optimized to improve the efficiency of an aircraft at all times during flight.

The different angles that can be altered to optimize a winglet's performance are designed to reflect changes in the aircraft's altitude, airspeed, pitch, and other external forces that exist on an air frame in flight. Figures 4 and 5 show the four main angles that affect a winglet's performance when mounted on a wing. The twist angle affects in what direction the wingtip vortex is shed. The larger the twist angle, the more outward (away from the aircraft) the wingtip vortex is directed. This helps in eliminating vortex interference for any objects downstream.¹² The toe angle exists to decrease the loads being felt by the

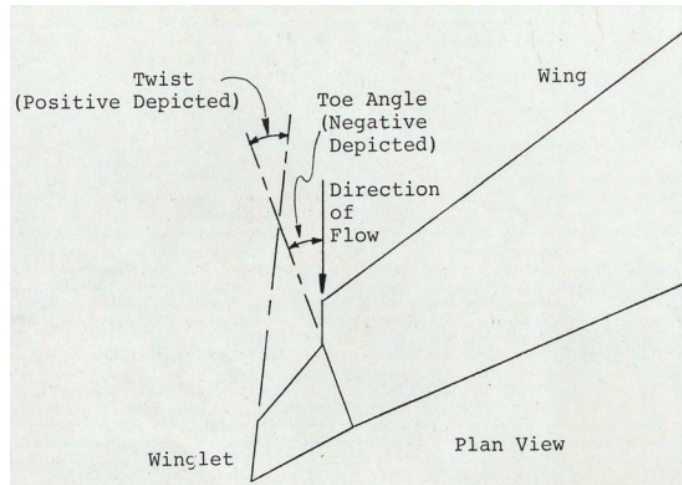


Figure 4: Winglet Angles¹³

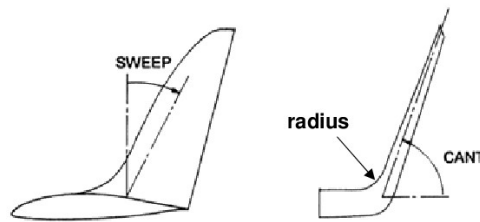


Figure 5: Winglet Angles¹⁴

wingtip to ultimately decrease any potential bending moments felt throughout the wing. The sweep angle, similarly to the twist angle, affects in what direction the wingtip vortex is shed. Instead of inward/outward, the sweep angle affects the upward/downward direction of the wingtip vortex shedding. The greater the sweep angle, the more downward the vortex is shed. This also exists to help eliminate potential vortex interference downstream. Lastly, the cant angle exists to decrease the magnitude of the vortex being shed.¹⁵ It is not designed to alter the direction of the vortex shedding. This is the main angle affecting the amount of drag being felt by the wings and plane as a whole.

The following analysis is carried out in order to find a system that can adjust one of

these angles. It consists of changing the cant angle of a simulated wing/winglet system. As stated, the cant angle has more of an effect on the magnitude of forces felt by an aircraft. It is because of this that this study focuses solely on the cant angle. The magnitudes of lift and drag are what affects aircraft performance the most. The cant angle is also the most easily variable and most easily measurable angle out of the four presented.

1.2.3 Data Analysis

In order to fully examine this idea, both computational fluid dynamics (CFD) and wind tunnel data are used in this experiment. The CFD model uses purely mathematical calculations and approximations in order to provide an ideal result of the lift and drag profiles. For CFD modeling, the 3D domain incorporates the changes in the forces due to both time and space within the flow field. It incorporates multiple factors relating to the accuracy of the model that are mentioned in Section 3.1.1 of this report. The use of CFD software is a common practice because of its accuracy and reliability. The CFD software that is used in this experiment is ANSYS. The CFD results are compared to the wind tunnel data to ensure the accuracy of the simulations.

The wind tunnel data collection method utilizes the total and static pressure of the flow to calculate the average force at a given location. This method works by gauging the static pressure at each pressure tap located both at the inlet of the test section and points on the test specimen. The difference between these pressures, along with the surface area and relative angle of attack, is used to calculate the total net force on the test specimen. This force can be non-dimensionalized for purposes of recreating the experiment using another method or another medium. For this experiment, the wind tunnel testing method is carried out in the Flotek 1440 Wind Tunnel located at the University of Vermont Fluids Lab. In this wind tunnel, the airfoil used has pressure taps built in that allow the lift and drag profiles

to be monitored. All of the calculations are non-dimensionalized. This is done to account for the two different methods and the error present because of small differences between the two.

In this design experiment, the principles of lift and drag are examined and an analysis of the winglet angle system is carried out. The lift and drag are calculated using the Flotek 1440 Wind Tunnel's manometer bank with pressure taps integrated into the airfoil. To create a more comprehensive understanding of the flow field, the system is then fully modeled using ANSYS CFD software and contour maps are created. This data is ultimately used to verify if the variable-angle winglet system is viable for further research and prototype development.

2 Models

2.1 Computational Test

2.1.1 Winglet Designs

Figures 6 - 10 show the five wing/winglet designs. The domain dimensions are presented in Section 4.1.1 after a domain study was done. The structure of each model is the same. The wing and winglet sections have the same profile. The only change between the models is their cant angle. The angles chosen are somewhat arbitrary. The two necessities were that a range from 0° to 90° needed to be tested and they needed to be somewhat evenly spaced out, with wide enough gaps between the five angles tested. Models with cant angles of 0° , 30° , 45° , 60° , and 90° were tested and are shown in the drawings below. The sizes on these drawings are also arbitrary. Because everything is being non-dimensionalized in the end, the actual sizes do not matter for the purposes of this experiment.

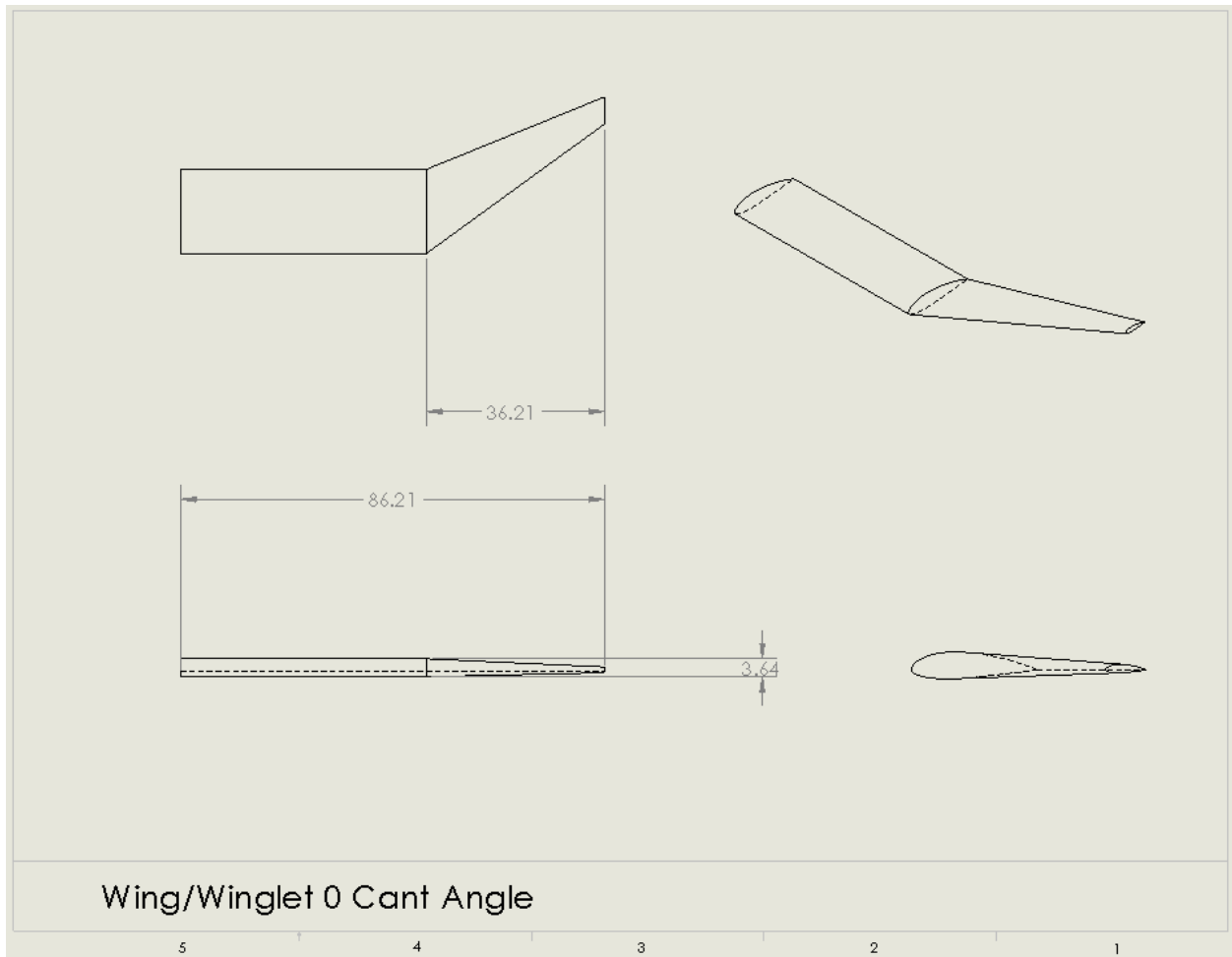


Figure 6: Winglet System with 0° Cant Angle

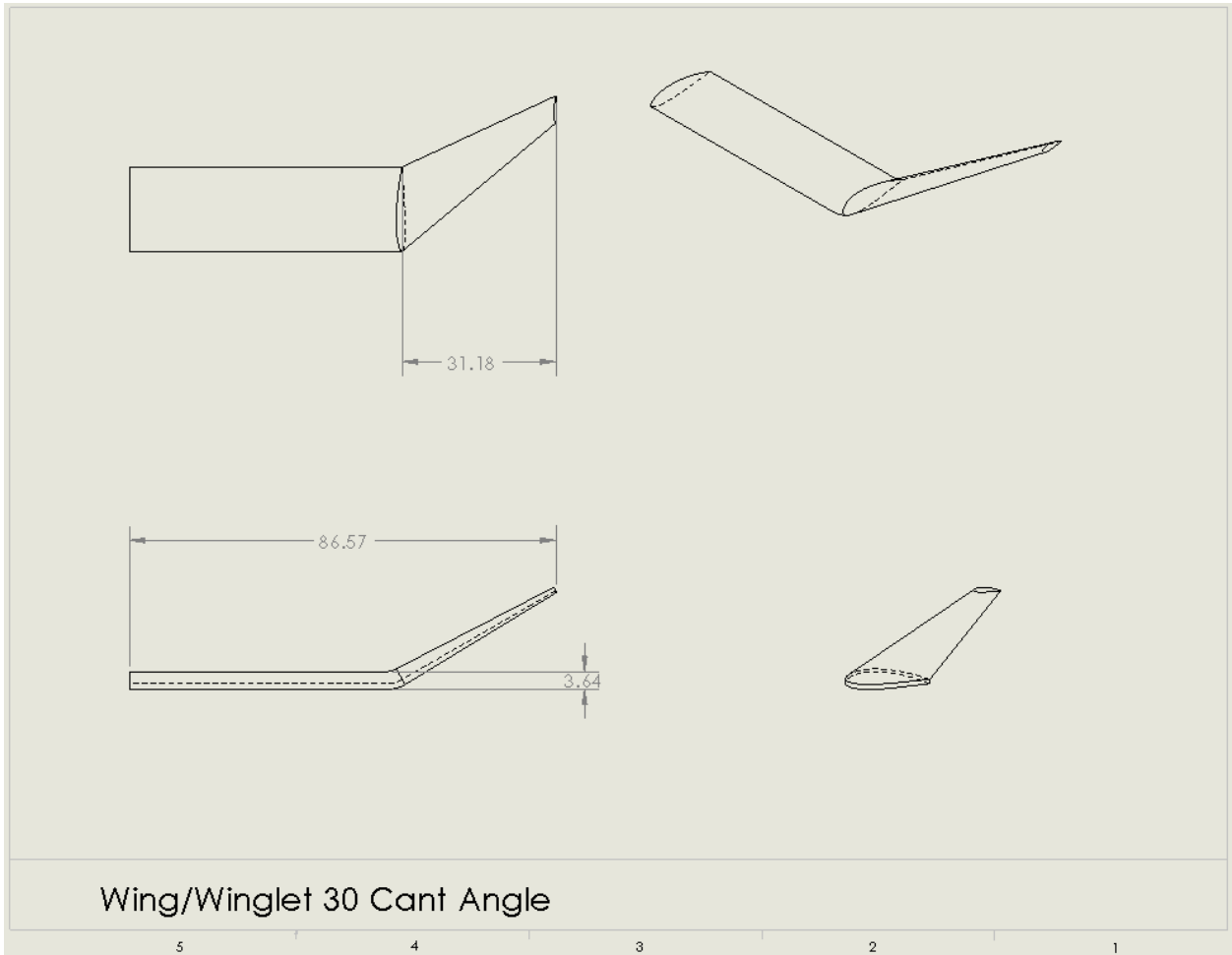


Figure 7: Winglet System with 30° Cant Angle

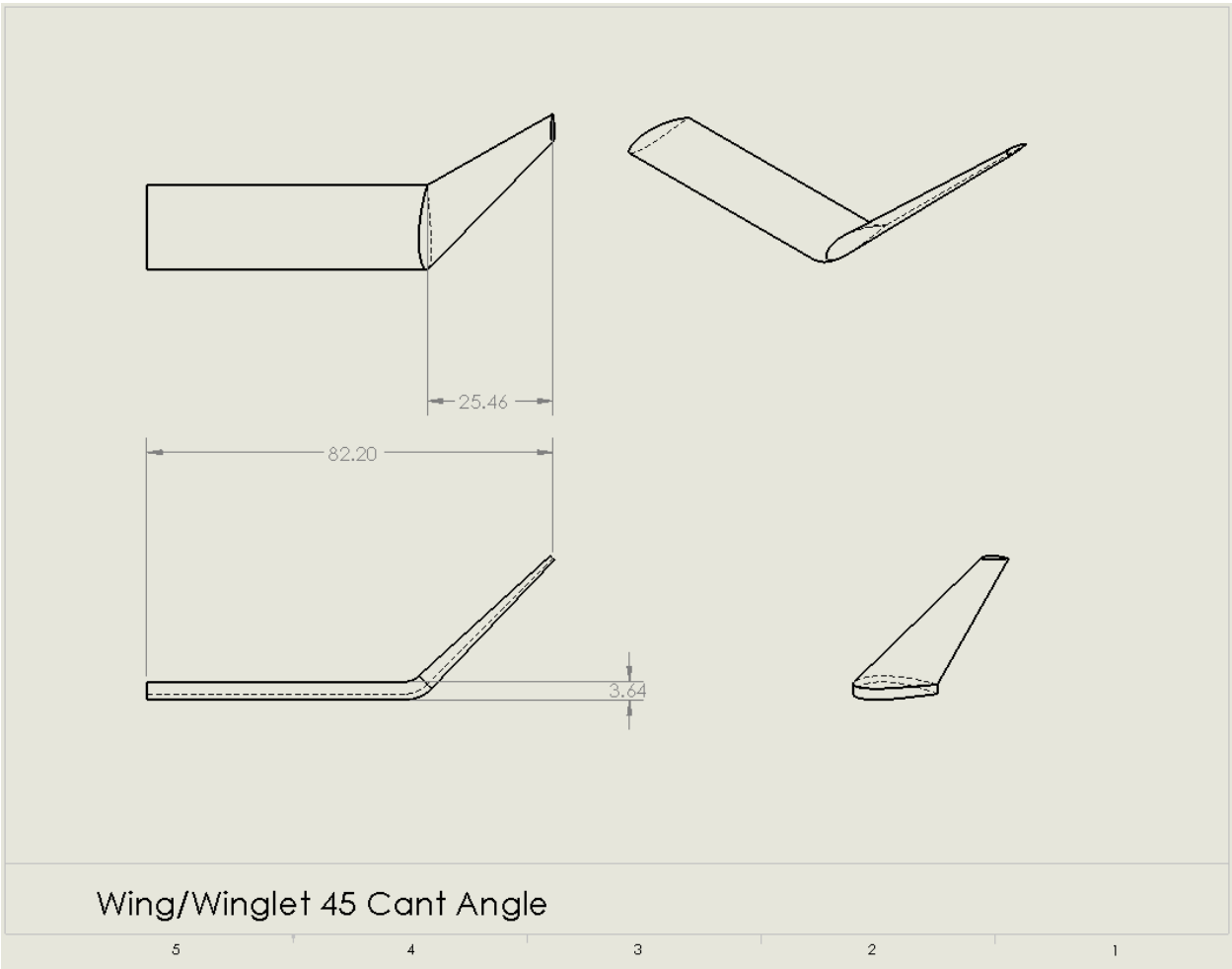


Figure 8: Winglet System with 45° Cant Angle

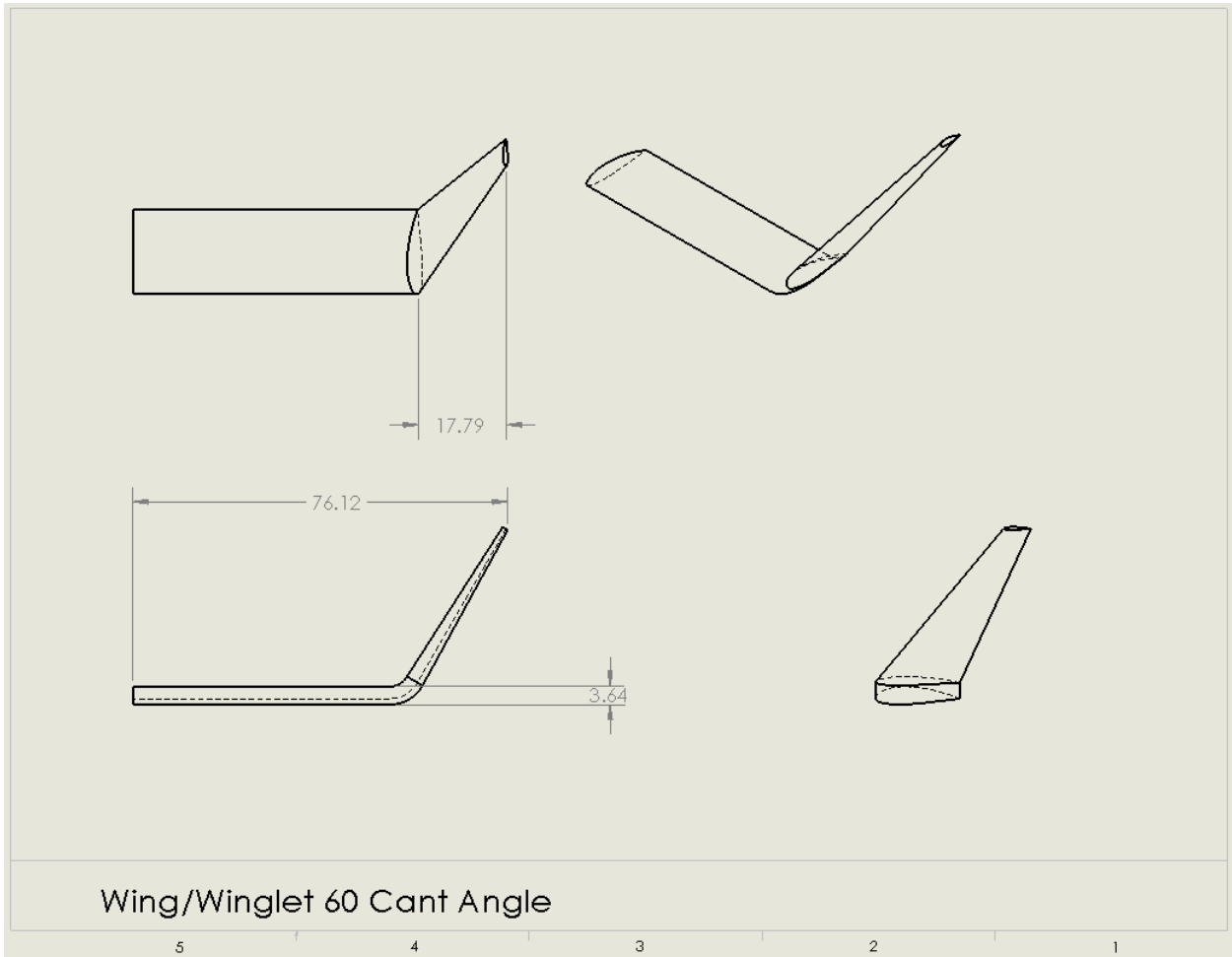


Figure 9: Winglet System with 60° Cant Angle

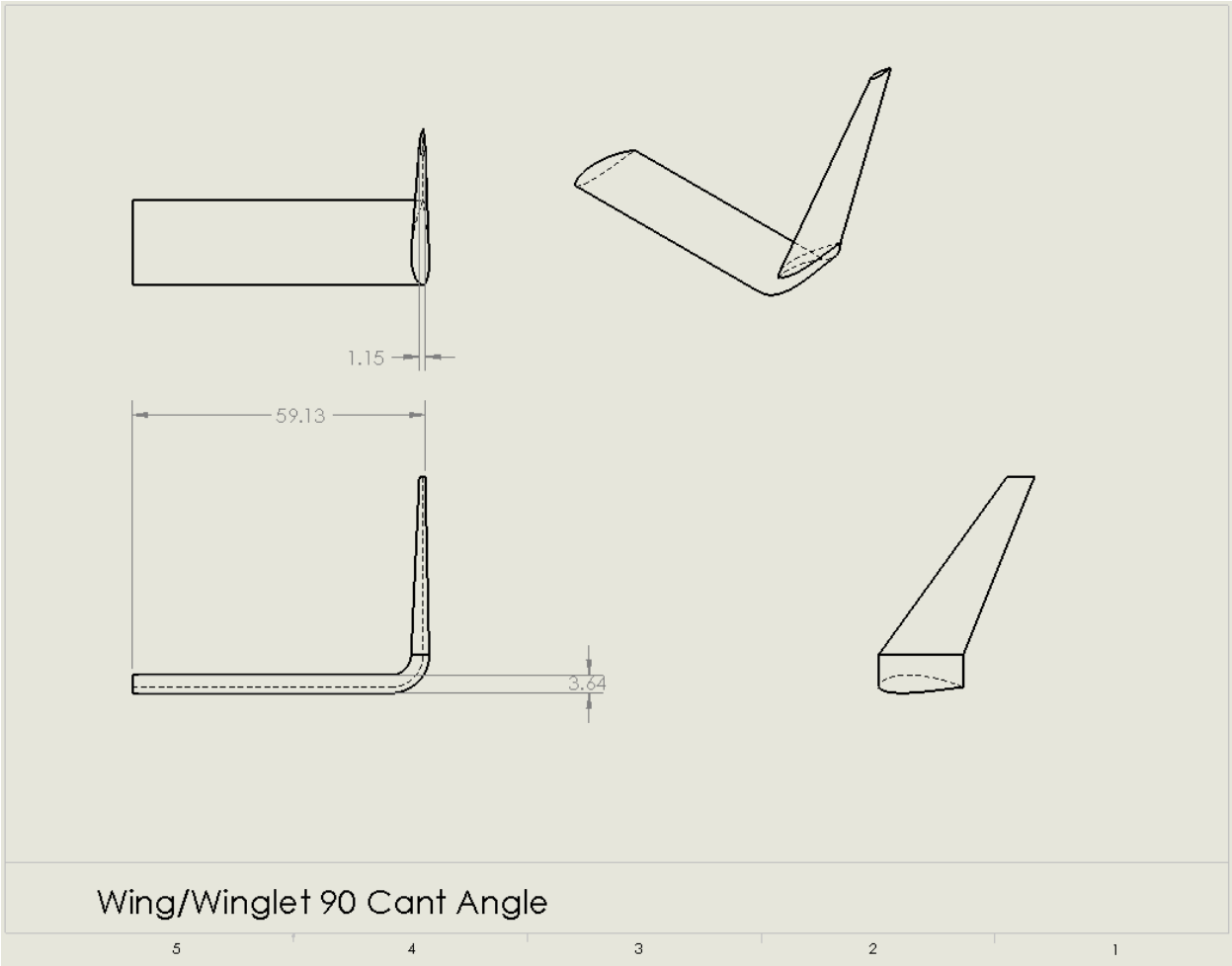


Figure 10: Winglet System with 90° Cant Angle

2.1.2 Physics Model

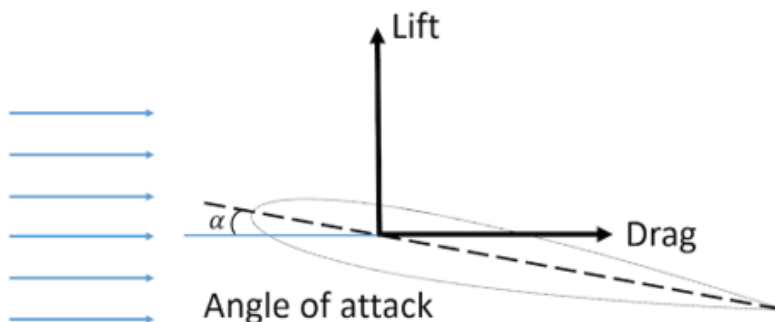


Figure 11: Physics Model¹⁶

The physics model in Figure 11 shows how the forces of lift and drag affect the cross section of a wing or winglet. These forces are measured using the CFD model for all of the 5 cant angle models. These forces are also found using wind tunnel methods on the airfoil provided. The implementation of this physics model defines the directionality of the lift and drag forces for the purposes of the CFD modeling and wind tunnel tests.

2.1.3 Domain & Boundary Conditions

The domain and boundary conditions of the 3D computational model show the structure of the domain and the boundary conditions. These figures contain the 0° cant angle wing, but all 5 wing/winglet systems will have the same domain and boundary. Figures 12 - 14 show the domain and boundary conditions. The breakdown of the domain is shown in more detail in the mesh study. The mesh study is located in Section 4.1.1. The numerical models are defined next. They are used by the solver of the CFD in the ANSYS modeling program.

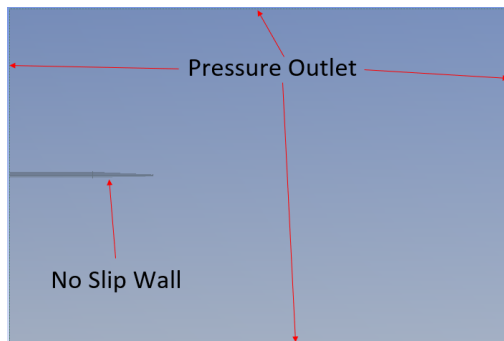


Figure 12: Front View

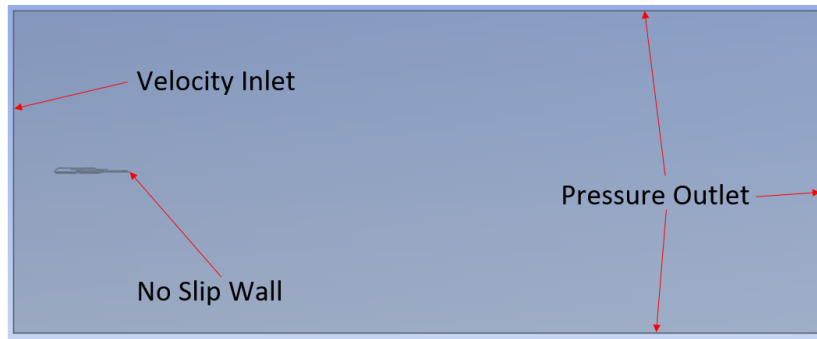


Figure 13: Right View

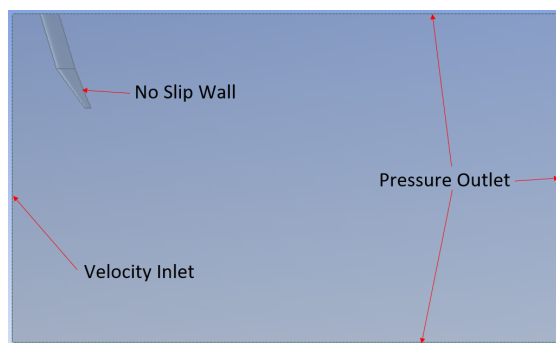


Figure 14: Top View

2.1.4 Numerical Models

The following numerical models are used for each test of this experiment:

- Solver:
 - Pressure-based
 - Steady-state
- Laminar flow
- No gravity
- Implicit formulation
- Spatial discretization:
 - Gradient: least-squares cell based
 - Flux Type: Roe FDS
 - Flow: 2nd Order Upwind

2.2 Wind Tunnel Test

The NACA2415 airfoil is used in the wind tunnel test and calculations. This airfoil, as can be seen in Figure 15, is a standard airfoil simulating an aircraft wing with 8 pressure taps on top of the wing and 8 on the bottom. The 16 total pressure taps allow for lift and drag calculations at each location and a total lift and drag force to be calculated. A 17th pressure tap located at the inlet of the test section of the wind tunnel provides upstream data and allows the pressure differences, and thus the forces, to be calculated. There is no particular reason the NACA2415 airfoil was chosen, only that it was readily available and provided for this project by the University of Vermont.

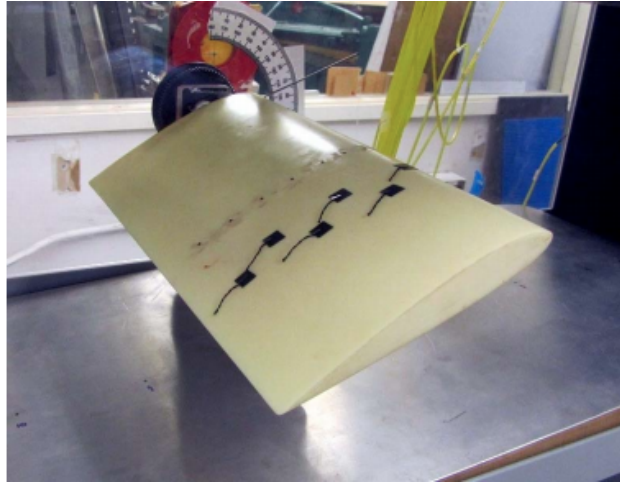


Figure 15: NACA2415 Airfoil

3 Methods & Measurements

3.1 Methods

3.1.1 Computational Test Methods

Computational modeling is done in order to examine the effects of a varying cant angle for the given airfoil profile. The above models are designed by taking the profile of the NACA2415 airfoil, extruding the profile, and adding a winglet at 5 different cant angles, whose values are previously provided. The size of the wing/winglet systems are designed arbitrarily with only relative dimensions being of utmost importance. The results are then non-dimensionalized to account for this. The size of the winglet is calculated using the dimensions outlined in Figure 16. Only the upper winglet is applied at varying cant angles, the lower winglet was ignored for the purposes of this experiment. The cross-section profile of the winglet matched that of the wing.

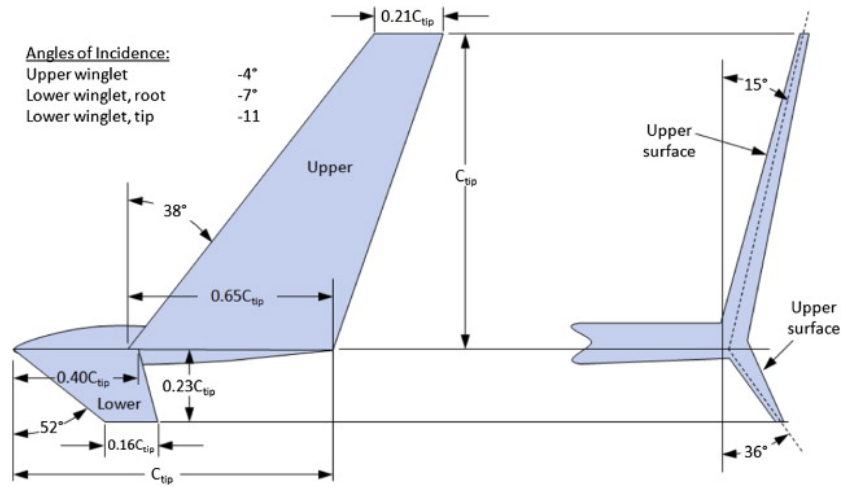


Figure 16: Winglet Dimensioning¹⁷

Once these five models are made, they are put into the domain that is shown in Section 4.1.1 in the domain study. Using ANSYS CFD software, the velocity profile of the flow downstream of the winglet system is visualized. In addition to visualizing the flow field with contour plots, raw data is taken across specific sections of the domain that show the changing lift and drag profiles. This model produces the ideal solution for the flow. Along with the raw experimental data, which has some random error, the data received from the CFD simulations proves crucial to visualizing the lift and drag profiles and determining if the variable-angle winglet system is effective or not.

In setting up the simulations, it is important to correctly identify the proper boundary conditions and operating conditions that are present in real time. Starting with the domain, it is essential that it be large enough to capture all of the important flow structures that will be present as a result of the wing/winglet geometries being subjected to the freestream flow. It is also key to have a fine enough mesh to capture all of the flow structures accurately and completely. An unrefined mesh leads to too much estimation in the domain and unreliable data. For this reason, the domain and grid study are carried out in Section 4.1.1.

After setting up the domain and boundary conditions, the specific models are formally defined and the solver schemes are set. The physics model, as shown in Figure 11 in Section 2.1.2, shows how the forces on the wing system are defined. It is important to understand the physics model before defining any other parameters. The physics model allows one to visualize the flow field before running tests. The numerical models, as displayed in Section 2.1.4 are chosen based on how the model should be calculated mathematically. The pressure-based solver is chosen because the flow is not being compressed. Despite having a Mach number greater than 0.3 at times, the only potential compression of the flow would occur at a stagnation point on the wing. On these models, there is one small stagnation point as shown in Figure 24 in Appendix 7.1. There is no shock effect and this stagnation point manifests as the pressure drag. A steady-state solver was chosen because the models are not changing in time. While multiple time points are tested, the change in the flow field with respect to time is not important. Multiple steady-state tests are run as a result.

In terms of the flow, a laminar flow model is chosen. Despite having traditionally turbulent Reynolds numbers ($Re > 4000$), the effects of the turbulence do not need to be captured. Only the total lift and drag forces need to be measured, not the specific pattern of the flow or the small eddy-currents and other effects of turbulence that occur. Because the Reynolds numbers and velocities are so high, gravity can be neglected. Implicit formulation is used to produce the most accurate information, and the spatial discretization mentioned in Section 2.1.4 is applied. These three discretizations are chosen because of the accuracy of the resulting information, the reliability of the model, and the ability for the model to complete in a reasonable amount of time.

When deciding on the Reynolds numbers to be tested, the velocities of the wind tunnel at 5 different power settings were considered as well as reconstructing real flight conditions. The specific speeds are found in Section 3.2.1. They are found using Equation 1 or a variation of

it, which can be found in Section 4.1.2. The final information about test cases can be found in Section 4.1.1 in Table 1. As stated, the Reynolds numbers are found using Equation 1, the velocities are found from wind tunnel data and flight conditions for passenger aircraft,¹⁹ and the densities and pitches of the aircraft. The characteristic length of the wind tunnel model is 0.1m and the characteristic length of a real aircraft is 2m.¹⁹ The final information of flight test conditions is seen in Table 1.

3.1.2 Wind Tunnel Test Methods

Wind tunnel testing and results are carried out in order to verify the validity of the computational model. In the ideal scenario, direct replicas of tested models would be produced. However in this experiment, data was taken from a previously tested experiment using the NACA2415 airfoil. The data is normalized in attempt to compare to the values of the results of the computational model. Figures 15 and 17 show the airfoil and the setup, respectively.



Figure 17: Flotek 1440 Wind Tunnel¹⁸

Using this model brings up another source of error when attempting to compare data. There is a slight geometrical difference between the NACA2415 airfoil and the airfoil tested

in the CFD model. To minimize this, the lift and drag coefficients of the winglet with 0° are tested and the data are compared to the NACA2415 airfoil. While the comparison is not perfect, the relationships and trends between the lift and drag coefficients are looked at in attempt to show that the trends carry over between the two. The trends between the two are the most important thing. If the trends are consistent across each testing method, then the conclusions made from the CFD model will accurately reflect the relationships between lift and drag for each winglet cant angle model.

For each test in the wind tunnel, the absolute pressure of the inlet of the test section is represented by Equation 2, as shown in the calculations in Section 4.1.2. Here, the manometer heights are taken into account as well as the atmospheric pressure. This value is used to find the inlet velocity of each test. Knowing the inlet velocity for each test allows for the calculations of lift and drag to be done. The inlet velocity of the wind tunnel is calculated in Equation 3 and is strictly dependent on the relationship between the heights of the fluid in the manometer tubes of the inlet and atmospheric pressure taps. It should be noted that the density of water is used because the density of the manometer fluid is approximately that of water. The pressure at each of the 16 other taps is found using Equation 4.

Knowing the heights of the manometers both at the inlet of the test section and at the measurement locations at each of the 16 other pressure taps, the relationship between these heights allows the pressures to be known at all 16+1 locations tested. These pressures, P_∞ and P_i , are important to calculating the total lift and drags force on the winglet system. So too are α , ϕ , and A. Equations 5 & 6 show how the lift and drag forces are calculated at each pressure tap. To normalize all of the calculations due to different velocities, etc., the lift and drag coefficients are calculated using Equations 7 & 8. The coefficients take into account the dynamic pressure and the wing surface area as shown in Equation 9, in order to non-dimensionalize the forces. Knowing the lift and drag forces calculated at each pressure

tap and the total lift and drag coefficients, the effect of the lift and drag can be mapped and compared to the values calculated using the CFD model. This is done to validate the accuracy of the CFD model.

3.2 Measurements

3.2.1 Computational Test Measurements

There were no direct measurements using the computational data. All of the computational data can be found in Sections 4.1.1 & 4.2.1 and Appendix 7.2.

3.2.2 Wind Tunnel Test Measurements

The specific wind tunnel measurements are taken and the drag coefficients at various angles of attack are calculated. These drag coefficients are located in Appendix 7.3 in Tables 12 and 13. A total of 16 measurements are taken along the top and bottom of the NACA2415 airfoil and a total drag force is calculated. Based on that calculated drag force, a drag coefficient is determined. This drag force that is determined is based on 5 different inlet velocities tested. The only values that are being compared to the computational data in this entire data set is the lift and drag coefficients at 0° angle of attack. Although these values are not consistent, the maximum percent error between the wind tunnel test and CFD model is 14%. This is an acceptable percent error for this specific test.

4 Calculations & Results

4.1 Calculations

4.1.1 Computational Test Calculations

This study consists of 10 simulations. The first 5 are to replicate the 5 wind tunnel tests. The second 5 are to model 5 different flight conditions. Table 1 shows all of the conditions that each of the 10 simulations are conducted at. As stated previously, the goal of this is to verify the simulations with the experimental data and model the conditions experienced over a normal flight. The data resulting from these experiments is analyzed and a conclusion is reached as to the effectiveness and practicality of a variable-angle winglet system. Table 1 is seen below:

Table 1: Test Conditions

Condition	Height (m)	Density ($\frac{kg}{m^3}$)	Length (m)	Re	U_∞ ($\frac{m}{s}$)	Pitch ($^\circ$)
Tunnel 1	0	1.225	0.1	$1.9 * 10^5$	23.0	0
Tunnel 2	0	1.225	0.1	$2.0 * 10^5$	24.2	0
Tunnel 3	0	1.225	0.1	$2.3 * 10^5$	27.8	0
Tunnel 4	0	1.225	0.1	$2.4 * 10^5$	29.0	0
Tunnel 5	0	1.225	0.1	$2.6 * 10^5$	31.4	0
Takeoff	0	1.225	2	$1.1 * 10^7$	80	0
Climb	$\approx 5,000$	0.74	2	$2.0 * 10^7$	200	+15
Cruise	$\approx 11,000$	0.4	2	$1.6 * 10^7$	300	0
Descent	$\approx 5,000$	0.74	2	$1.8 * 10^7$	175	+3
Landing	0	1.225	2	$1.3 * 10^7$	70	0

Before the simulation process, a domain and grid study is completed. The studies include simulations run on the 0° winglet model, as it is the model used in all 10 simulations referenced previously. Completing these studies will provide the most accurate domain and mesh for the solver. For each study, the coefficients of lift and drag are monitored. The domain is

extended downstream, with a predetermined width, height, and upstream distance, until the percent change for each variable is below 1%. The width, height, and upstream distance are estimated initially and, through the resulting figures, do not appear to be sources of error. This conclusion is made from the fact that there does not appear to be any large velocity gradient emanating from those boundaries, also seen in Appendix 7.1. The results are shown in Table 2 and Figure 18.

Table 2: Extended Domain Study Results

Extended Domain Size	C_D	C_L
4	0.060	0.599
5	0.098	0.659
6	0.111	0.702
7	0.121	0.711
8	0.127	0.718
9	0.131	0.721
10	0.132	0.722

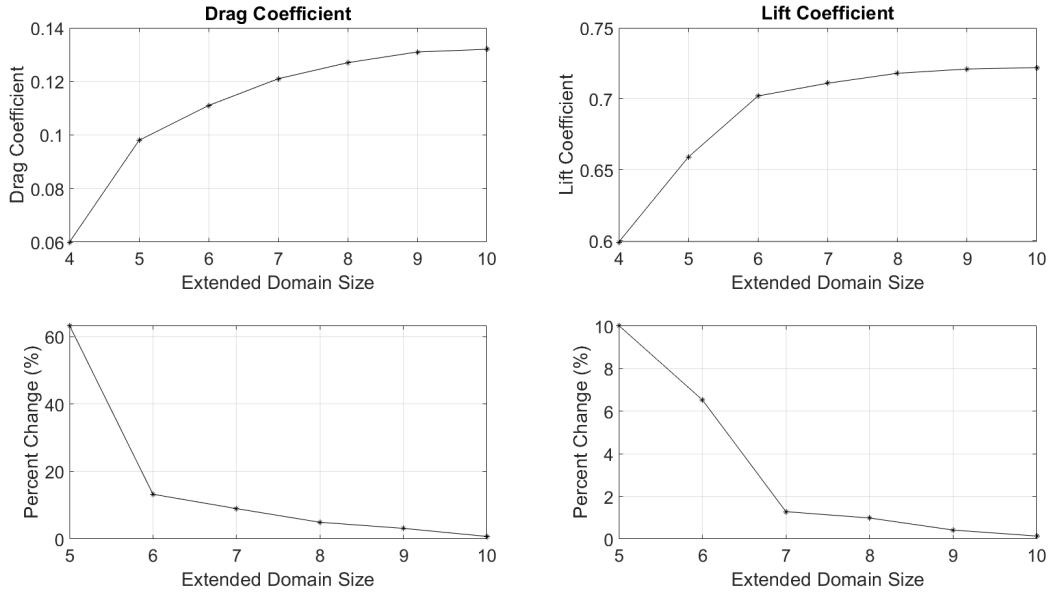


Figure 18: Extended Domain Study Results

C_L & C_D for the CFD model are taken over the entire surface of the model. The grid study is carried out in a very similar manner, with the same variables monitored. In this study, the number of finite volumes are found. The mesh must be fine enough to not affect the result with mathematical error. The results of this study are shown in Table 3 and Figure 19. A convergence plot can be found in Figure 22 in Section 4.2.1.

Table 3: Grid Study Results

Finite Volumes	C_D	C_L
109,600	0.062	0.666
185,364	0.099	0.702
226,777	0.115	0.710
254,008	0.127	0.717
532,889	0.132	0.721
846,322	0.132	0.722
912,028	0.132	0.722

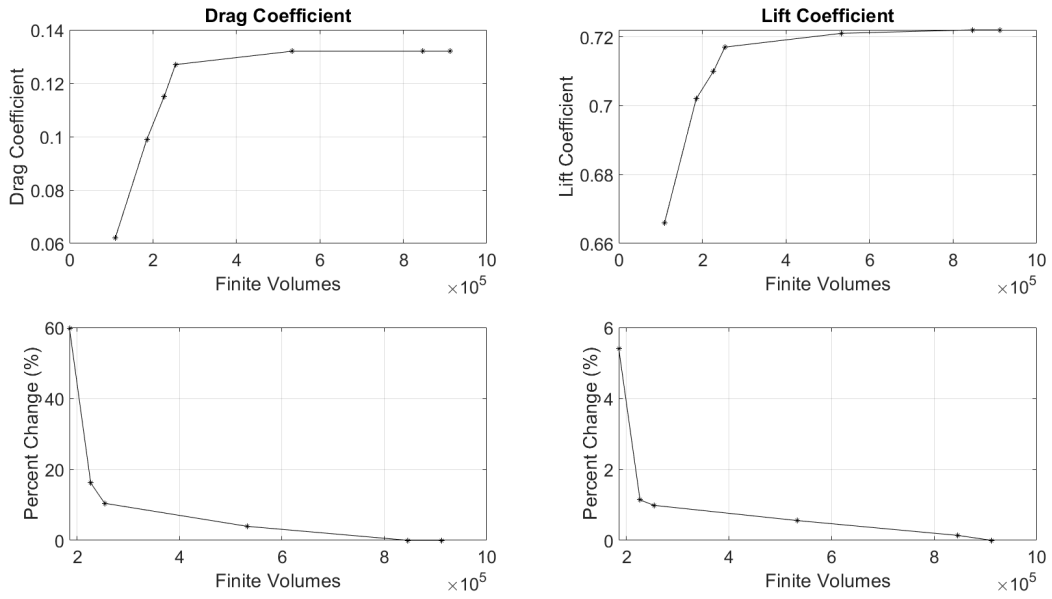


Figure 19: Grid Study Results

With the domain and grid studies completed, as well as the models determined, the simulations can be run with minimal mathematical error. The final result of the domain study produces the domain shown in Figure 20:

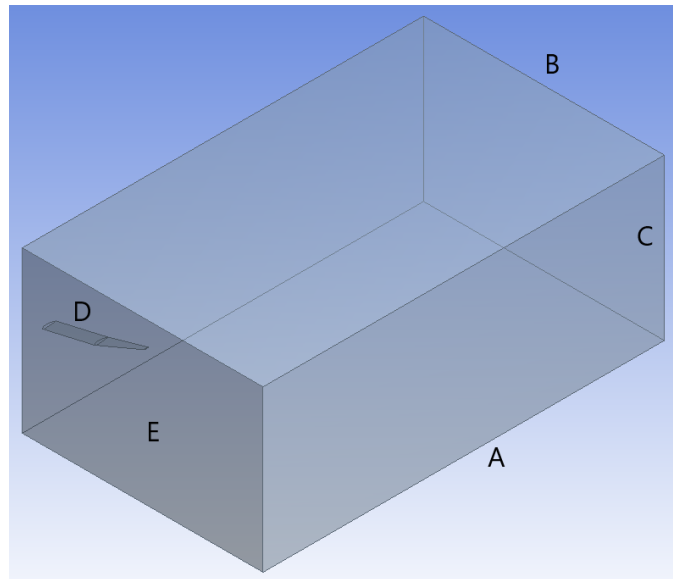


Figure 20: Domain to be Tested

Notes:

- Edge A & 3 parallel: 225 divisions, 5 bias factor towards wing
- Edge B & 3 parallel: 75 divisions, 10 bias factor towards wing
- Edge C & 3 parallel: 75 divisions, 5 bias factor centered at wing
- D: all wing structures are no-slip walls
- Face E: velocity inlet
- All other faces: pressure outlets
- Body sizing: 0.015 m

4.1.2 Wind Tunnel Test Calculations

$$Re = \frac{\rho_a U_\infty D}{\mu} \quad (1)$$

Equation 1 is used to calculate the Reynolds number of the flow. A variation of it is used to find the velocity when the Reynolds number is known.

$$P_\infty = P_{atm} - \rho_w g(h_\infty - h_{atm}) \quad (2)$$

Equation 2 is used to calculate the pressure at the inlet of the test section.

$$U_\infty = \sqrt{\frac{2\rho_w g(h_\infty - h_{atm})}{\rho_a}} \quad (3)$$

Equation 3 is used to calculate the velocity at the inlet of the test section.

$$P_i = P_{atm} - \rho_w g(h_i - h_{atm}) \quad (4)$$

Equation 4 is used to calculate the the pressure at each location on the test specimen.

$$F_L = -(P_i - P_\infty)\cos(\alpha - \phi)A \quad (5)$$

Equation 5 is used to calculate the lift force at each location on the test specimen.

$$F_D = -(P_i - P_\infty)\sin(\alpha - \phi)A \quad (6)$$

Equation 6 is used to calculate the drag force at each location on the test specimen.

$$C_L = \frac{F_L}{q_\infty S} \quad (7)$$

Equation 7 is used to calculate the lift coefficient of the test specimen.

$$C_D = \frac{F_D}{q_\infty S} \quad (8)$$

Equation 8 is used to calculate the drag coefficient of the test specimen.

$$q_\infty = \frac{1}{2} \rho_a U_\infty^2 \quad (9)$$

Equation 9 is used to calculate the dynamic pressure of the flow.

4.2 Results

4.2.1 Computational Test Results

The results of the computational simulations include the velocity fields and the lift and drag forces/coefficients. For each model, multiple simulations are run at various angles of attack and at various windspeeds. The model containing the 0° cant angle is run for all 10 simulations outlined in Table 1. The first 5 simulations are run to ensure reliability of the model by relating the results to the wind tunnel results. For these simulations, the initial velocities are set under sea level conditions. Table 4 shows the lift and drag coefficients that are calculated over the entire solid. There is no mathematical calculation done to find these. All are calculated fully within the ANSYS CFD program.

Table 4: Lift and Drag Coefficients for 0° Cant Angle Model

Test Number	Re	C_D	C_L
1	$1.9 * 10^5$	0.125	0.732
2	$2.0 * 10^5$	0.132	0.722
3	$2.3 * 10^5$	0.135	0.718
4	$2.4 * 10^5$	0.134	0.719
5	$2.6 * 10^5$	0.132	0.744

The comparison of the lift and drag coefficients are presented in Tables 10 and 11 in Section 4.2.2. These comparisons show the likeness of the simulations to the tests conducted in the wind tunnel. The results are further explained in Section 4.2.2. From here, each additional flight condition is tested.

Following the completion of the first 5 simulations and the affirmation of the validity of the model, all 5 cant angle models are run for the last 5 simulations listed in Table 1. For these simulations, the coefficients of lift and drag are examined. They are analyzed because the relationship between the two is key as to which cant angle can be considered optimal. During takeoff and cruise, the least amount of total drag is desired ($(C_D)_{min}$). For climb, the highest ratio of lift to drag is desired ($(\frac{C_L}{C_D})_{max}$). For descent, it is very dependent on the specific scenario. For the purpose of this experiment, the lowest ratio of lift to drag is desired ($(\frac{C_L}{C_D})_{min}$). This is the case because this would result in the most rapid descent, which would be most optimal, provided lift is still maintained. Lastly, for landing, the highest drag force is desired ($(C_D)_{max}$).²⁰

In simulating for takeoff, cruise, and landing at level flight, the aforementioned conditions in Table 1 are used. Because the pitches are the same for these cases, the relationships between the drag and lift coefficients will be the same (i.e. the highest $C_{D,L}$ and the lowest $C_{D,L}$ will occur at the same angle for all 3 tests). The varying velocities and air densities will only affect the specific lift and drag magnitudes, which are not directly being studied. Only the relationship between lift and drag is being looked at. Thus, only one set of test conditions need to be run to determine the lift and drag relationships for takeoff, cruise, and landing. An example of the flow development can be seen in Figure 21, which shows slices of the domain of the 0° cant angle model for level cruise. The coefficients of lift and drag on these models are displayed in Table 5.

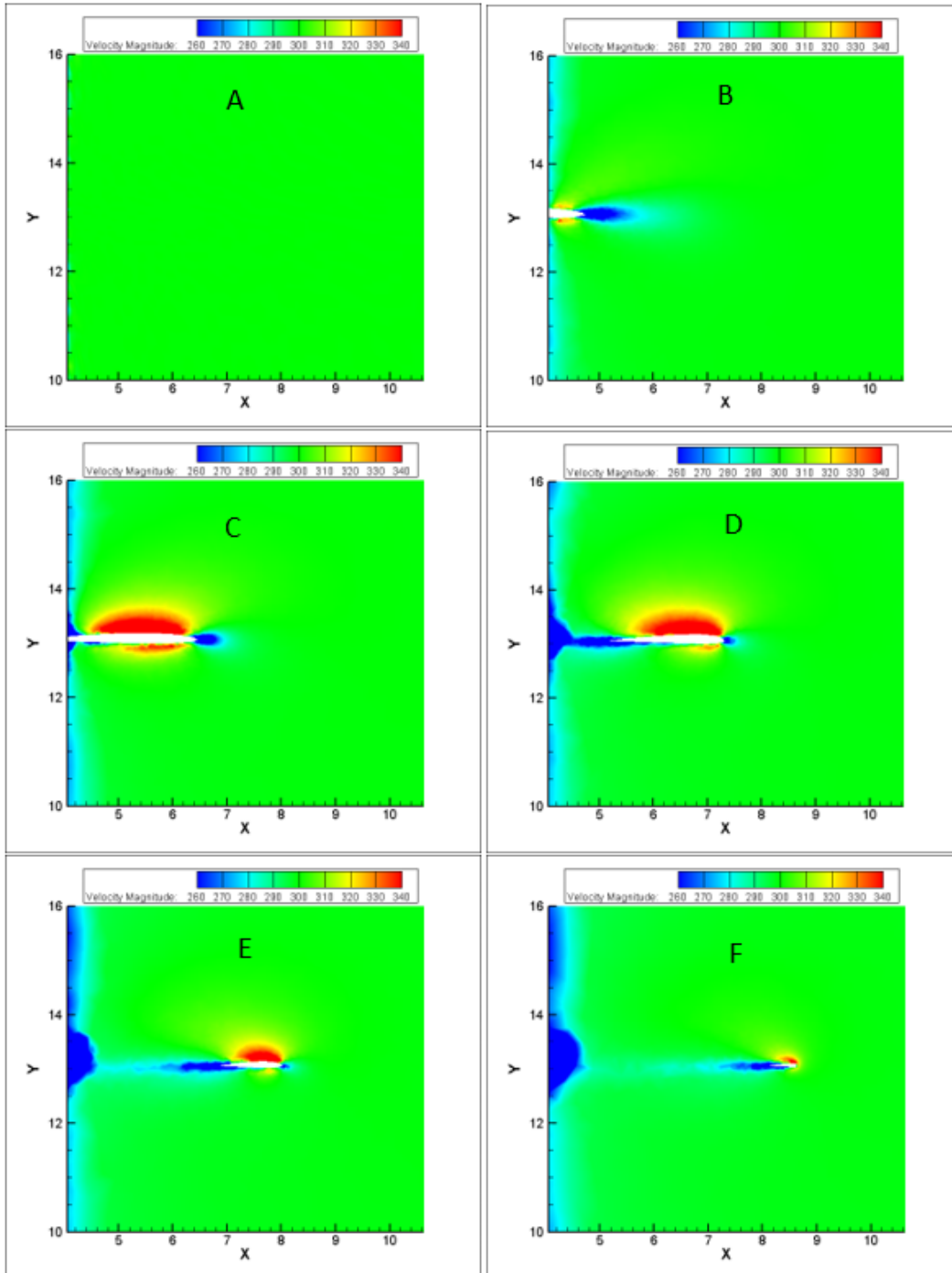


Figure 21: 0° Cant Angle Flow Visualization for Level Cruise

Table 5: Lift and Drag Coefficients for Cruise

Cant/Sweep Angle ($^{\circ}$)	C_D	C_L
0	0.136	0.735
30	0.111	0.731
45	0.123	0.722
60	0.128	0.720
90	0.130	0.722

From this table, it can be seen that the model with a cant angle that produces the lowest drag coefficient is the 30° winglet. This system cuts down most effectively on both friction drag and aerodynamic drag (vortex shedding). For the takeoff and cruise scenarios, a winglet with 30° cant angle will be most ideal out of the 5 models simulated. For landing, the winglet angle producing the highest C_D will be ideal as previously stated. This is the 0° cant angle model. This angle does not cut down on vortex shedding. If one wants to cut down on vortex shedding, the 90° angle model has a similar C_D . All of these values are recorded in Table 8.

Figure 21 shows the flow path that is consistent throughout all of these simulations. The presence of high relative velocity on the top surface of the wing and low relative velocity on the bottom surface of the wing shows that lift is still maintained. This velocity difference results in a static pressure difference that sees the net force on the wing directed upwards. This shows that throughout the models, lift is still maintained. A couple of trends to consider in looking at the data from these tests, is 1) the addition of a non- 0° cant angle winglet greatly decreases the drag, and 2) the greater the cant angle, the larger the drag coefficient becomes. Having a 0° of pitch, the drag profiles for takeoff, cruise, and landing follow these same trends. For ascent and descent, more simulations are conducted.

For ascent and descent, the optimal winglet angle is once again found through simulations. The values in Table 1 are used to conduct the simulations. Each of the 5 cant angle models

is tested, which results in $\frac{C_L}{C_D}$ relations. These relations, as discussed previously, show which cant angle out of the 5 tested is considered most optimal. For these simulations, because the pitch is non-zero, the velocity of the flow is broken down by component. For climb, with a pitch of $+15^\circ$ and a velocity magnitude of $200\frac{m}{s}$, the horizontal component of velocity is $193.2\frac{m}{s}$ and the vertical component is $51.76\frac{m}{s}$. Similarly, for descent, there is a pitch of $+3^\circ$ and a velocity magnitude of $175\frac{m}{s}$. The horizontal component of this is $174.8\frac{m}{s}$ and the vertical component is $9.16\frac{m}{s}$. The lift and drag coefficients from the ascent and descent simulations are shown in Tables 6 & 7, respectively.

Table 6: Lift and Drag Coefficients for Ascent

Cant/Sweep Angle ($^\circ$)	C_D	C_L	$\frac{C_L}{C_D}$
0	0.202	0.732	3.62
30	0.184	0.734	3.99
45	0.185	0.741	4.01
60	0.187	0.736	3.94
90	0.199	0.716	3.60

From this table, it is seen that the cant angle model with the highest $\frac{C_L}{C_D}$ is the 45° model. This system is the most effective at providing the greatest ratio of lift to drag for the given conditions. Deduced from this is the fact that, based on these simulations, the 45° cant angle model is most ideal for ascent, based on the 5 models simulated. Because of pitch and/or altitude differences, the relationships between C_D & C_L differ between ascent, descent, and level flight.

The lift and drag coefficients for descent are then found. Instead of a pitch angle of $+15^\circ$, there is now a pitch angle of $+3^\circ$. Despite the aircraft going in a downward direction, there is still a positive relative pitch angle during descent. This is done to help slow the aircraft as it gets closer to the ground. During this type of flight, more of the surfaces of the aircraft are subjected to the flow and so the additional air friction helps slow the plane.

During descent, the aircraft slows from about $300\frac{m}{s}$ to about $80\frac{m}{s}$.²⁰ There is also a lot of variability in the rate of descent for a generic commercial aircraft. This simulation aims to target the average rate of descent at an average speed between cruise and landing speeds. From various sources,^{1,8,20} the average descent pitch and speeds are determined to be $+3^\circ$ at $175\frac{m}{s}$, respectively. The CFD simulations are done under these flight conditions. The actual results varies dramatically and algorithms need to be made to find the optimal angle over the entire descent if this product is implemented. For the purposes of this experiment, only the aforementioned conditions are simulated. Table 7 shows the results of these simulated tests:

Table 7: Lift and Drag Coefficients for Descent

Cant/Sweep Angle ($^\circ$)	C_D	C_L	$\frac{C_L}{C_D}$
0	0.152	0.732	4.81
30	0.122	0.739	6.06
45	0.136	0.733	5.39
60	0.142	0.730	5.14
90	0.150	0.725	4.83

Based on these results, the cant angle models with the lowest $\frac{C_L}{C_D}$ are 0° and 90° . Much like the landing scenario the optimal angle is either 0° or 90° , depending on if the vortices being shed by the 0° cant angle winglet prove problematic. If they do, then the 90° cant angle winglet would provide nearly the same amount of lift to drag, but the vortex magnitudes would be much lower. Their respective values of 4.81 and 4.83 do not provide enough of a difference for significant alterations in performance to occur. Table 8 displays a summary of the optimal cant angles found for all flight conditions studied.

Table 8: Cant Angle Summary

Flight Condition	Optimal Winglet Cant Angle
Takeoff	30°
Ascent/Climb	45°
Cruise	30°
Descent	0°, 90°
Landing	0°, 90°

Figure 22 shows an example of the convergence of the continuity and the x, y, and z velocities. It shows the residuals that were the highest for all tests run. This occurred during the ascent simulation for the model with a cant angle of 90°. In this figure, there is evidence of no divergence throughout the 1,000 iterations of the domain.

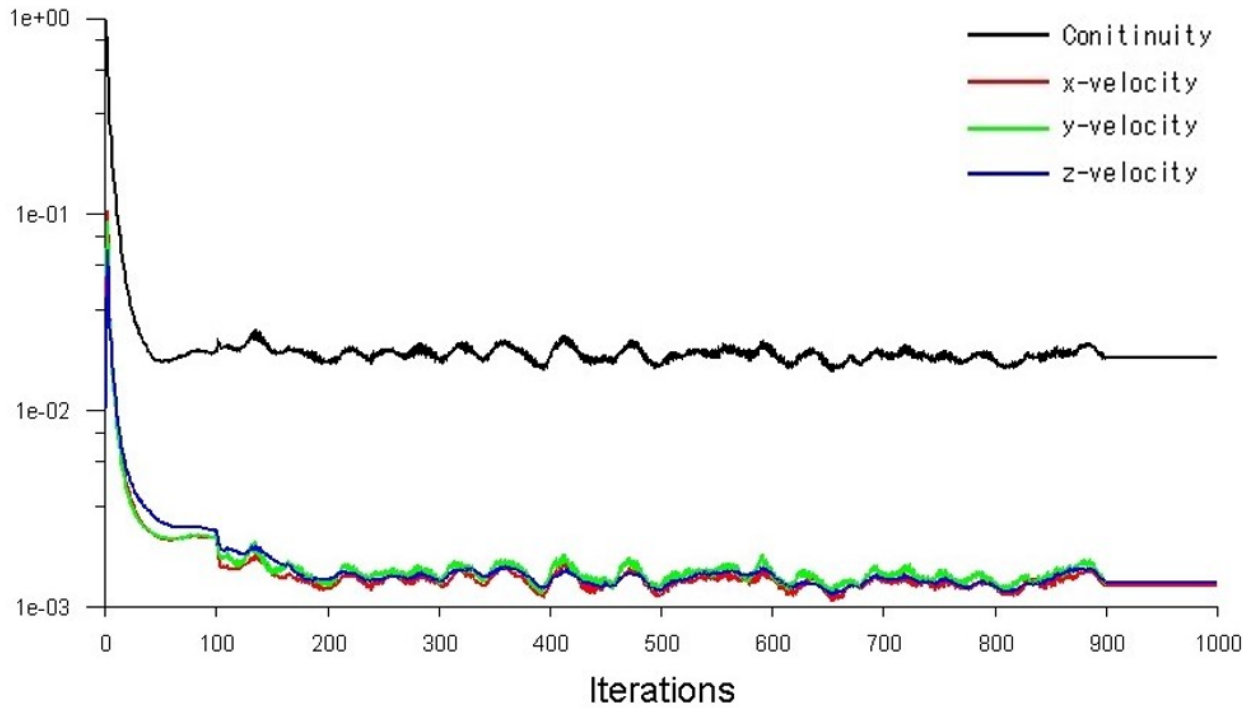


Figure 22: Convergence for 90° Cant Angle Model Ascent Simulation

4.2.2 Wind Tunnel Test Results

Table 9: Summary of C_D & C_L in Wind Tunnel Tests

Re	C_D	C_L
$1.9 * 10^5$	0.140	0.849
$2.0 * 10^5$	0.155	0.844
$2.3 * 10^5$	0.163	0.833
$2.4 * 10^5$	0.152	0.829
$2.6 * 10^5$	0.144	0.851

The results for the wind tunnel testing are found in Appendix 7.3, with the most important information being displayed in Table 9. The lift and drag coefficients show resemblance to the computational testing, as shown in Tables 10 & 11, which compare the calculated lift and drag coefficients between the two tests.

Table 10: Comparison of C_D Between Two Testing Methods

Re	Wind Tunnel Test	Computational Test	Percent Error (%)
$1.9 * 10^5$	0.140	0.125	10.7
$2.0 * 10^5$	0.155	0.132	14.8
$2.3 * 10^5$	0.163	0.135	17.2
$2.4 * 10^5$	0.152	0.134	11.8
$2.6 * 10^5$	0.144	0.132	8.33

Table 11: Comparison of C_L Between Two Testing Methods

Re	Wind Tunnel Test	Computational Test	Percent Error (%)
$1.9 * 10^5$	0.849	0.732	13.8
$2.0 * 10^5$	0.844	0.722	14.5
$2.3 * 10^5$	0.833	0.718	13.8
$2.4 * 10^5$	0.829	0.719	13.3
$2.6 * 10^5$	0.851	0.744	12.6

Tables 10 and 11 show an average percent error of 11-14%. While this is higher than the optimal 5%, it should be recognized that the drag coefficient is consistently lower for the computational test and the lift coefficient is consistently higher. Based on the geometries of the models, as shown in Sections 2.1.1 & 2.2, this error can be attributed to the slight geometrical differences in the each of the models. The geometry of the CFD model has a winglet with a 0° cant angle whereas the NACA2415 airfoil used in the wind tunnel has no winglet at all. While this systematic error is certainly not ideal, there is minimal random error present in the comparison. The trends seen in the wind tunnel test ($(C_{D,L})_{max,min}$ and $(\frac{C_L}{C_D})_{max,min}$) are also seen in the CFD simulations. From here, it is valid to say that data produced by the CFD is reliable. If re-ran, the CFD model should run the wing geometry without the winglet to eliminate some of this error.

5 Conclusions

In the simulations carried out and the experiment completed, the aerodynamic and physical effects of several different winglet models are tested. The goal of this study is to determine if a variable-angle winglet system is viable for potential prototyping. It is considered viable if the optimal wing angle changes significantly at different flight levels, pitches, and air speeds. Despite having idealized wing geometries, no fuselage or engine configurations, the data recorded from this study shows that the optimal winglet angle will change over the course of one flight. As a sanity check, from a practical sense it checks out that the 30° geometry is best for cruise, since most fixed winglets on commercial aircraft have a cant angle around 30° . Also, it makes sense that the 0° cant angle geometry would have the highest drag, since implementing cant angle winglets was initially done to account for this problem.

The overall data recorded shows that the effects of lift and drag do vary significantly

for all flight conditions based on the winglet angle. These results are presented in Tables 5 - 7, and summarized in Table 8. The data includes consideration of the flight conditions, and the variability in optimal winglet angles demonstrates the benefit of a proposed system. Assuming the controls would be programmed, the control system could take real time data and adjust the angles accordingly. This would account not only for flight conditions, but also weather, other air traffic, and any variable that might affect the aircrafts performance not considered in this study. The completion of these experiment reveals the usefulness of the product and provides adequate reasoning for further research regarding implementing a variable-angle winglet system.

In a potential system, many more variables than just the cant angle of a winglet system should be looked at. The sweep, toe, and twist angles should be considered and every variable in the geometry of each wing should be taken into account. This additional research and implementation will come at a cost, as fully installed testing and modelling will need to be done and the addition of this system will cost more than a fixed winglet system otherwise would. The potential benefits that would outweigh the drawbacks would be safer flights, decreased emissions, and savings on fuels costs for each flight. The addition of these systems would increase aircraft efficiency and ultimately allow for faster, longer flights to be profitable.

6 Future Work

Upon conclusion of these experiments, there are more critical things that need to be done to move forward the process of researching a potential variable-angle winglet system. The next steps to be taken are as follows:

1. **3D model printing:** The next step in verifying the computational model more di-

rectly is to implement identical wind tunnel tests for each of the 5 model tested. To do this, 3D printed models of each wing/winglet system need to be made, ideally with capabilities that would allow for pressure taps to be placed throughout the wing and winglet just like the NACA2415 airfoil.

2. **Wind tunnel testing:** Once the models are made, tests would need to be run in the wind tunnel to more accurately identify the parameters of lift and drag that were compared in this experiment. A more accurate data set would provide better proof of validity of the CFD model. Tests must be verified with CFD and physical tests in order for results to be considered definitive.
3. **Finite element analysis:** Once a standard prototype design is decided, the forces taken from the CFD model need to be applied to an FEA model. This is to be done to ensure structural stability of the winglet system. The FEA model needs to have the range of stability necessary for all optimal flight conditions.
4. **Cost benefit analysis:** Once a design is decided upon, a cost analysis needs to be done to ensure that the device is worth the cost of production. The analysis will need to take into account the material cost, production cost, and cost of implementation on future aircraft. The design will need to incorporate the correct material, production, and manufacturing processes.

7 Appendix

7.1 Pressure Map Along Wing Cross-section

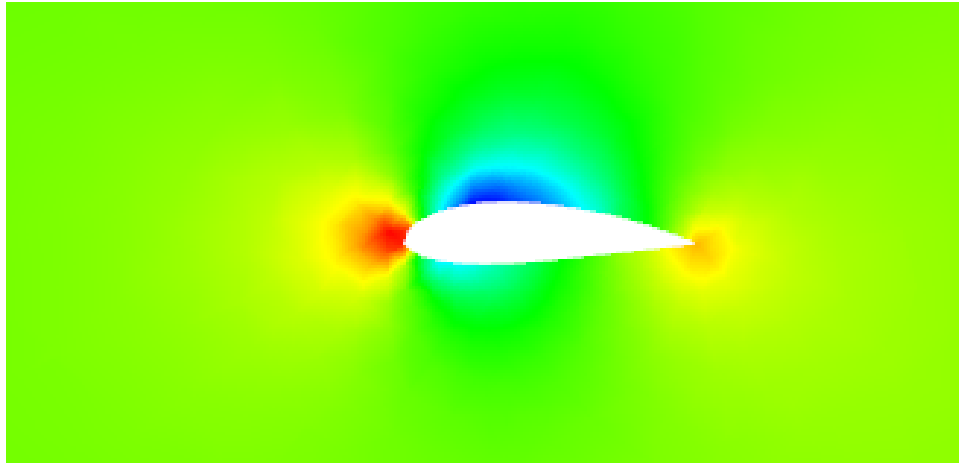


Figure 23: Pressure Difference Along Wing Cross-section

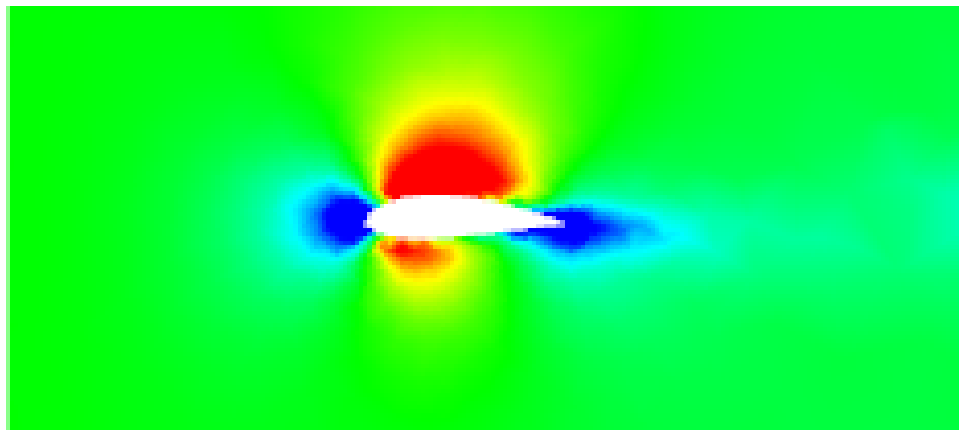


Figure 24: Velocity Difference Along Wing Cross-section

7.2 Computational Journal File

```
# encoding: utf-8
# Release 19.2
SetScriptVersion(Version="19.2.120")
templatel = GetTemplate(TemplateName="Fluid Flow")
system1 = templatel.CreateSystem()
geometry1 = system1.GetContainer(ComponentName="Geometry")
geometry1.Edit()
Save(Overwrite=True)
meshComponent1 = system1.GetComponent(Name="Mesh")
meshComponent1.Refresh()
mesh1 = system1.GetContainer(ComponentName="Mesh")
mesh1.Edit()
Save(Overwrite=True)
setup1 = system1.GetContainer(ComponentName="Setup")
fluentLauncherSettings1 = setup1.GetFluentLauncherSettings()
fluentLauncherSettings1.SetEntityProperties(Properties=Set(Dimension="ThreeD", EnvPath={}))
setup1.Edit()
setup1.SendCommand(Command='(cx-gui-do cx-set-list-tree-selections "NavigationPane*List_Tree1"
(list "Setup|General"))(cx-gui-do cx-set-list-tree-selections "NavigationPane*List_Tree1"
(list "Setup|Materials"))(cx-gui-do cx-set-list-tree-selections "NavigationPane*List_Tree1"
(list "Setup|General"))')
setup1.SendCommand(Command='(cx-gui-do cx-set-list-tree-selections "NavigationPane*List_Tree1"
(list "Setup|General"))(cx-gui-do cx-activate-item "NavigationPane*List_Tree1")')
setup1.SendCommand(Command='(cx-gui-do cx-set-list-tree-selections "NavigationPane*List_Tree1"
(list "Setup|General"))(cx-gui-do cx-set-list-tree-selections "NavigationPane*List_Tree1"
(list "Setup|Materials"))')
setup1.SendCommand(Command='(cx-gui-do cx-set-list-tree-selections "NavigationPane*List_Tree1"
(list "Setup|Materials"))(cx-gui-do cx-activate-item "NavigationPane*List_Tree1")')
setup1.SendCommand(Command='(cx-gui-do cx-set-list-tree-selections "NavigationPane*List_Tree1"
(list "Setup|Materials"))(cx-gui-do cx-set-list-tree-selections "NavigationPane*List_Tree1"
(list "Setup|Materials|Fluid"))(cx-gui-do cx-set-list-tree-selections "NavigationPane*List_Tree1"
(list "Setup|Materials|Solid"))(cx-gui-do cx-set-list-tree-selections "NavigationPane*List_Tree1"
(list "Setup|General"))')
setup1.SendCommand(Command='(cx-gui-do cx-set-list-tree-selections "NavigationPane*List_Tree1"
(list "Setup|General"))(cx-gui-do cx-activate-item "NavigationPane*List_Tree1")')
setup1.SendCommand(Command='(cx-gui-do cx-set-list-tree-selections "NavigationPane*List_Tree1"
(list "Setup|General"))')
setup1.SendCommand(Command='(cx-gui-do cx-activate-item "ToolBar*View Tools*autoscale")')
Save(Overwrite=True)
Reset()
```

7.3 Wind Tunnel Data

Table 12: Drag Coefficient Results

Re	Angle of Attack ($^{\circ}$)									
	-4	-2	0	2	4	6	8	10	12	14
19000	0.367	0.191	0.140	0.154	0.164	0.173	0.186	0.191	0.223	0.259
19700	0.307	0.256	0.155	0.149	0.171	0.171	0.180	0.195	0.201	0.233
22500	0.326	0.246	0.163	0.159	0.159	0.171	0.190	0.187	0.211	0.262
24000	0.352	0.255	0.152	0.152	0.166	0.170	0.185	0.190	0.220	0.244
26000	0.344	0.250	0.144	0.163	0.160	0.177	0.196	0.180	0.215	0.239

Table 13: Lift Coefficient Results

Re	Angle of Attack ($^{\circ}$)									
	-4	-2	0	2	4	6	8	10	12	14
19000	0.499	0.592	0.849	0.887	0.921	0.824	0.752	0.714	0.698	0.654
19700	0.487	0.587	0.844	0.879	0.922	0.830	0.750	0.716	0.696	0.655
22500	0.501	0.599	0.833	0.890	0.909	0.836	0.749	0.722	0.691	0.661
24000	0.492	0.599	0.829	0.893	0.911	0.833	0.755	0.720	0.688	0.660
26000	0.496	0.603	0.851	0.881	0.925	0.827	0.744	0.728	0.702	0.665

8 Acknowledgements

The following all contributed assistance to this project:

- **Emily Ryan:** helped develop initial prototypes
- **Sam Perry:** helped model final prototype
- **Dr. William Louisos:** provided guidance over the entire project
- **Dr. John Novotny:** helped narrow down final thesis idea
- **Dr. Darren Hitt:** assisted initial thesis planning
- **Vermont Advanced Computing Core:** offered for testing on their system
- **University of Vermont:** provided software and facilities for all testing

References

- [1] Guerrero, J., Sanguineti, M., & Wittkowski, K. (2018) CFD Study of the Impact of Variable Cant Angle Winglets on Total Drag Reduction, *Aerospace*, 5-6. DOI: 10.3390/aerospace5040126.
- [2] Mattingly, J. D., Boyer, K. M., & von Ohain H. (2016), *Elements of Propulsion: Gas Turbines and Rockets*, 38-39, ISBN: 978-1-62410-371-1
- [3] [Picture of Airplane Wing]. (n.d.). Retrieved from <https://www.grc.nasa.gov/www/k-12/airplane/cruise.html>
- [4] Flechner, S. G., Jacobs, P. F., & Whitcomb, R. T. (1976), A High Subsonic Speed Wind-Tunnel Investigation of Winglets on a Representative Second-Generation Jet Transport Wing, 13-14, Retrieved from <https://ntrs.nasa.gov/archive/nasa/casi.ntrs.nasa.gov/19760019076.pdf>
- [5] Flechner, S. G., Jacobs, P. F., & Whitcomb, R. T. (1976), A High Subsonic Speed Wind-Tunnel Investigation of Winglets on a Representative Second-Generation Jet Transport Wing, 16, Retrieved from <https://ntrs.nasa.gov/archive/nasa/casi.ntrs.nasa.gov/19760019076.pdf>
- [6] Guerrero, J., Sanguineti, M., & Wittkowski, K. (2018) CFD Study of the Impact of Variable Cant Angle Winglets on Total Drag Reduction, *Aerospace*, 12-14. DOI: 10.3390/aerospace5040126.
- [7] [Picture depicting in-flight forces]. (n.d.). Retrieved from <https://www.grc.nasa.gov/www/k-12/airplane/cruise.html>

- [8] van Leeuwen, B., Capelle, C., Casanova, A. M., Finn, S., & Guo, S. (2017), An Overview of Commercial Aircraft 2018 - 2019, *Aviation Research (AR)*, 7-162, Retrieved from <https://www.dvbbank.com/~media/Files/D/dvbbank-corp/aviation/dvb-overview-of-commercial-aircraft-2018-2019.pdf>
- [9] [Picture Depicting Vortex Generation]. (n.d.). Retrieved from https://www.wikiwand.com/en/Wingtip_device
- [10] de Mattos, B. S., Macedo, A. P., & da Silva Filho, D. H. (2003), Considerations about Winglet Design, *Journal of Aircraft*, 4-6 <https://doi.org/10.2514/6.2003-3502>
- [11] Takenaka, K., Hatanaka, K., Yamazaki, W., & Nakahashi, K. (2008), Multidisciplinary Design Exploration for a Winglet, *Journal of Aircraft*, 45(5), 1601-1602, <https://doi.org/10.2514/1.33031>
- [12] Moore, T. T. (1976), The Effect of Winglet Twist and Toe Angle on the Drag of a High Aspect Ratio Wing” *Retrospective Theses and Dissertations*, 17-19, Retrieved from <https://pdfs.semanticscholar.org/ffd0/c1ad2dd8ceb271504e69dc09acf32f755762.pdf>
- [13] Moore, T. T. (1976), The Effect of Winglet Twist and Toe Angle on the Drag of a High Aspect Ratio Wing” *Retrospective Theses and Dissertations*, 5, Retrieved from <https://pdfs.semanticscholar.org/ffd0/c1ad2dd8ceb271504e69dc09acf32f755762.pdf>
- [14] Queirolo, M. A. (2018), Impact of Morphing Winglets on Aircraft Performance, 51-52, Retrieved from <https://repository.tudelft.nl/islandora/object/uuid:86a76d02-70f8-4468-a805-40ab4900b1a0/datastream/OBJ/download>
- [15] Abdelghany, E. S., Khalil, E. E., Abdellatif, O. E., & Elhariry, G. (2016), Air Craft Winglet Design and Performance: Cant Angle Effect, *Journal of*

Robotics and Mechanical Engineering Research, 1(3), 32-33, Retrieved from <http://verizonaonlinepublishing.com/ROBOTICSPDF/JournalofRoboticsandMechanicalEngineeringResearch14.pdf>

- [16] Braaten, M. E., & Gopinath, A. (2011), Aero-Structural Analysis of Wind Turbine Blades With Sweep and Winglets: Coupling a Vortex Line Method to ADAMS/AeroDyn, 2-3, DOI: 10.1115/GT2011-45904
- [17] Gudmundsson, S. (2014), *General Aviation Aircraft Design*, Butterworth-Heinemann, <https://doi.org/10.1016/C2011-0-06824-2>
- [18] [Picture of Wind Tunnel]. (2017). Retrieved from <https://vtdigger.org/2017/10/06/uvm-opens-phase-one-104-million-stem-facility/>
- [19] Mattingly, J. D., Boyer, K. M., & von Ohain H. (2016), *Elements of Propulsion: Gas Turbines and Rockets*, 49-50, ISBN: 978-1-62410-371-1
- [20] Mattingly, J. D., Boyer, K. M., & von Ohain H. (2016), *Elements of Propulsion: Gas Turbines and Rockets*, 60-64, ISBN: 978-1-62410-371-1